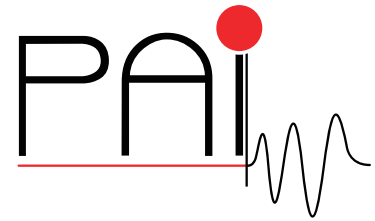


Research Network FWF S105

# Photoacoustic Imaging in Medicine and Biology



<http://pai.uibk.ac.at>

---

## Photoacoustic Tomography of Small Animals and Organs

M. Holotta, R. Esterhammer,  
P. Torbica, J. Völkl, C. Kremser,  
W. Jaschke, H. Grossauer,  
M. Haltmeier, O. Scherzer, R. Nuster,  
G. Paltauf, P. Burgholzer

June 2009

Original version: M. Holotta and H. Grossauer,  
Photoacoustic Tomography of Small Animals and Organs  
(Extended abstract, April 2009)

PAI Report No. 13

---

**FWF**

Der Wissenschaftsfonds.





# Photoacoustic Tomography of Small Animals and Organs

Markus Holotta, Regina Esterhammer, Pavle Torbica, Jakob Völkl, Christian Kremser, Werner Jaschke  
Innsbruck Medical University, Austria

Harald Grossauer, Markus Haltmeier, Otmar Scherzer  
University of Innsbruck, Austria

Robert Nuster, Günter Paltauf  
Karl-Franzens-University Graz, Austria

Peter Burgholzer  
Research Center for Non Destructive Testing GmbH (RECENDT), Austria

Keywords: photoacoustic imaging, tomography, integrating detectors, mammography, contrast agents

June 16, 2009

## 1 Introduction

Photoacoustic imaging (PAI) is becoming a major tool for preclinical studies owing to its unique property of combining aspects of optical and ultrasound imaging. Its potential for in-vitro and in-vivo imaging has been demonstrated both in photoacoustic tomography (PAT) setups and in photoacoustic microscopy. (Xu and Wang 2006; Kruger et al. 1995).

Moreover, PAI is considered a new screening technique and novel fields of biomedical applications are identified. Challenging questions in medical applications related to early cancer diagnosis and cancer treatment are of particular interest, as well as investigations of disease progression in thoroughly controlled small animal studies.

The aim of the present work is to evaluate the potentials of PAI for breast cancer imaging in-vitro and in-vivo. For in-vitro studies, biopsy and surgical specimen will be used. For in-vivo studies, an established mouse model will serve as a biological model for the development of breast cancer in human beings.

Current gold standard in breast cancer diagnosis is X-ray mammography with the disadvantage of ionising radiation and a rather high rate of false positive findings, resulting in an additional risk of cancer induction and unnecessary biopsies or even surgery. Thus, the differentiation of benign from malignant lesions is of utmost importance. In patients, ultrasound,

MRI and even PET scanning are commonly used to evaluate suspicious lesions detected by mammography. Still, some lesions cannot be classified as benign or malignant even by using sophisticated multimodality imaging. Photoacoustic tomography has the potential to improve visualization of breast cancer. In addition, PAT allows for non-invasive measurement of tissue oxygenation in-vivo, which can be used for the detection of pathologic tissue as well as for guiding or monitoring novel therapies.

In addition, nano particulate contrast materials can be visualized by PAT (Wang et al. 2004; De La Zerda et al. 2008). Contrast enhanced PAT may provide additional information on tissue characteristics. The identification of biological molecular markers for diagnosis and determination of therapy response for various diseases is currently a wide and active field of research. It has been shown previously that photoacoustic imaging in principle is capable to provide images of biological tissue where contrast is based on molecular differences within the tissues.

## 2 Principles of PAI

### 2.1 Physical Fundamentals of Medical Imaging

In PAI, a sample is illuminated by a short pulse of radiation, for example, a laser pulse. The energy of the laser pulse penetrates the sample and is absorbed inside. The amount of energy locally absorbed depends

on the spatially varying absorption coefficient. The absorption of energy results in local heating of the sample, which in turn causes the sample to expand. The duration of the pulse is much shorter than the thermal diffusion time, and therefore the thermal expansions causes a pressure wave to emanate from the sample. The temporal evolution of the pressure wave can be measured outside the sample. By using a back-projection or other reconstruction algorithm, the initial pressure, that is the pressure distribution induced by the laser pulse, can be computed. Since this initial pressure distribution is directly related to the local absorption coefficient, information about the inner structure of the sample is achieved.

Sonography (Ultrasonography, US) is an imaging modality which is applied in organ morphology, functional diagnostics as well as in therapy. Ultrasonic waves emitted by the ultrasonic probe are totally or partially reflected on boundary layers of the tissue. The higher the difference in density the higher reflection of sound. Penetration depth and resolution directly depend on the frequency of sound. The higher the sound frequency the better the resolution but the lower the penetration depth into the tissue (Thelen 2007).

One of the oldest imaging systems is radiography. The major disadvantage of this technique is the utilization of ionizing radiation. The spatial structures inside the body are projected onto a detector surface. Structures which lie on top of each other therefore are merged to one image (Heywang-Köbrunner and Schreer 2003).

Magnetic resonance imaging (MRI) is based on the physical effect of nuclear magnetic resonance of hydrogen protons. MRI uses no ionizing radiation however there is a risk stemming from the strong static magnetic field and the high frequency magnetic field. MRI provides higher soft tissue contrast and spatial resolution than radiography or sonography (Ewen 1998).

## 2.2 Experimental Setup for Photoacoustic Imaging

In our setup, the measurement of the pressure wave is performed by a Mach-Zehnder interferometer acting as an *integrating line detector* (Burgholzer et al. 2005; Paltauf et al. 2007b), see Fig. 1. A beam splitter splits a HeNe laser into two beams – the *reference beam* and the *measurement beam*. Both beams pass through a water tank and are brought to interference after the tank. In order to provide better acoustic coupling, the sample is put into the water tank close to the measurement beam. Laser pulses from an optical parametric oscillator (Continuum Surelite OPO Plus) pumped by a frequency tripled Q-switched Nd:YAG laser (Continuum Surelite 10 II, repetition frequency 10 Hz, pulse duration 5 ns) are fired at the sample.

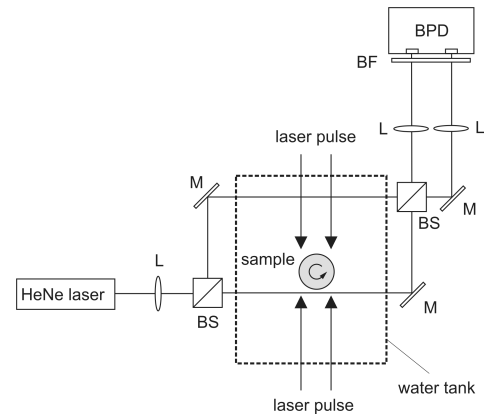


Figure 1: Experimental setup. L...lens, BS...beam splitter, M...mirror, BF...bandpassfilter, BPD...balanced photo detector

The pressure waves emanating from the sample lead to local changes in the refractive index of the water, causing the phase of the measurement beam to shift relative to the reference beam. When the two laser beams interfere, the phase shift causes oscillations in the intensity of the combined beam, which are measured by a photo detector (Thorlabs PDB120A) and recorded on a digital oscilloscope (LeCroy Waverunner 64Xi). Such a measurement is repeated numerous times as the sample is moved around the measurement beam.

Magnetic Resonance Imaging (MRI) was performed on standard 1.5T clinical whole body systems (Magnetom Avanto, Siemens, Erlangen, Germany) using a linear polarized small-loop receive coil (inner diameter 28 mm). For imaging of the ex-vivo mouse heart a T1 weighted 3D spoiled gradient-echo sequences (3D FLASH) was used with the following parameters: TR=32 ms, TE=16 ms, flip angle=50°, receive bandwidth: 50 Hz/pixel, slab thickness: 12 mm, number of slices: 20, effective slice thickness: 600  $\mu\text{m}$ , acquisition field of view (FOV): 25 mm x 50 mm, acquisition matrix 108x256, pixel spacing: 195  $\mu\text{m}$  x 195  $\mu\text{m}$ , number of averages: 4, total acquisition time: 4 min 37 s.

Ultrasound images were made with Philips iU 22 device. For acquisition of all images a linear-transducer was used: L17-5 MHz. For acoustic coupling the heart of the mouse was embedded in a gel pad.

X-ray images were made with GE-mammography-device Senograph 2000D. The detector pixel has dimensions of 100  $\mu\text{m}$  x 100  $\mu\text{m}$ . All images were made in magnification mode (1,9 fold) and under following conditions: kV:22, mAs:6, Anode: Molybdenum, Filter: Molybdenum.

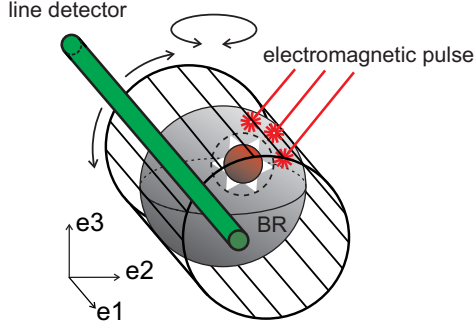


Figure 2: PAI with line detectors

### 2.3 Mathematical Modeling of Photoacoustic Imaging using Integrating Line Detectors

For ease of presentation we assume the water tank to be of infinite size. Then the pressure  $p(\vec{x}, t) : \mathbb{R}^3 \times \mathbb{R} \rightarrow \mathbb{R}$  in the water tank solves the wave equation

$$\frac{\partial^2 p}{\partial t^2} - \Delta p = 0$$

with initial condition

$$p(\vec{x}, 0) = u(\vec{x}), \quad \frac{\partial p}{\partial t}(\vec{x}, 0) = 0,$$

see (Xu and Wang 2006; Scherzer et al. 2009). Here  $u : \mathbb{R}^3 \rightarrow \mathbb{R}$  is the initial pressure distribution to be reconstructed, that is, the pressure induced by the laser pulse. We assume that the path of the measure beam is a line located at  $\vec{x}' \in \mathbb{R}^2$  and pointing into direction  $\mathbf{e}_1 := (1, 0, 0)$ , compare Fig. 2. Our data from one measurement are then proportional to

$$\bar{p}(\vec{x}', t) := \int_{\mathbb{R}} p(x_1, \vec{x}', t) dx_1.$$

It can be shown (Scherzer et al. 2009) that  $\bar{p}$  solves the following equation

$$\frac{\partial^2 \bar{p}}{\partial t^2} - \Delta \bar{p} = 0$$

with initial condition

$$\bar{p}(\vec{x}', 0) = \bar{u}(\vec{x}'), \quad \frac{\partial \bar{p}}{\partial t}(\vec{x}', 0) = 0,$$

where

$$\bar{u}(\vec{x}', t) := \int_{\mathbb{R}} u(x_1, \vec{x}', t) dx_1.$$

By measuring  $\bar{p}$  for many points  $\vec{x} \in \Gamma$ , with  $\Gamma \subset \mathbb{R}^2$  being a curve around the sample, we can reconstruct a *projection image*  $\bar{u}$  of the sample. By rotating the sample in small angle increments, and acquiring a projection image for each angle, we can reconstruct the three-dimensional structure of the sample.

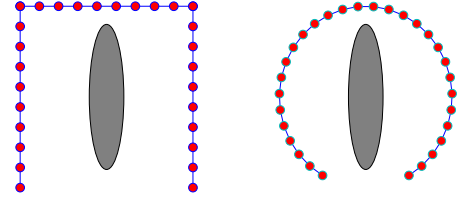


Figure 3: Special scan geometries: *U-scan* (left) and *C-scan* (right). The red dots depict the positions of the measurement laser beam

### 2.4 Scan Geometry and Reconstruction

The algorithm used for reconstructing the projection images depends strongly on the shape of the curve  $\Gamma$ , along which the measurements are performed. For arbitrary curves, *time reversal* can be used, see (Burgholzer, Matt, Haltmeier, and Paltauf 2007). Formulas of *back-projection* type give exact reconstructions for special detector geometries, or at least approximative reconstructions for arbitrary detector configuration, see (Burgholzer, Bauer-Marschallinger, Grün, Haltmeier, and Paltauf 2007). These algorithms are computationally expensive and the results often show artifacts. More efficient algorithms based on eigenfunction expansion exist for special curve geometries, as shown in Fig. 3. If the detector positions are located along a straight line—as for example on each side of a U-scan—an exact reconstruction can be achieved by a Fourier transform method, see (Köstli et al. 2001). For a circular configuration of detector positions—as given in a C-scan—an exact reconstruction formula is given by means of a Hankel transform, see (Haltmeier et al. 2007).

A comprehensive study of all three reconstruction methods (time reversal, back-projection, and eigenfunction expansion) can be found in (Hristova et al. 2008).

Relating to Fig. 3 two remarks are in order:

1. In practice we move the sample around the laser beam (and not vice versa), since the interferometer reacts very sensitive to mechanical influences.
2. For the reconstruction to be stable and exact (at least in theory) the sample has to be completely contained within the convex hull of  $\Gamma$ .

In our measurements we exclusively perform U-scans and/or C-scans, since the positioning of the sample in these cases is quite easy, and reconstruction is fast and robust. To keep the effects of acoustic attenuation of the pressure wave small, it would be advantageous to guide the measurement beam as close to the sample as possible. Therefore the detection curve should ideally be a slightly enlarged version of the

silhouette of the sample. This would require a sophisticated positioning system, since the detection curve would be different for each orientation of the sample. Further we would have to revert to the slower and more artifact prone time reversal reconstruction.

For mechanical reasons we cannot measure all around the sample, because at some point the mounting of the sample would block the measurement laser beam. Therefore we have no measurement data for the lower side of the U-scan, resp., the lowermost part of the C-scan. The corresponding *limited view problem* is discussed in (Paltauf et al. 2007a).

Once all the projection images have been computed, the reconstruction process proceeds as follows: Let  $\bar{u}_\theta(y, z)$ ,  $\theta \in [0, \pi]$ , denote the projection images acquired with the sample rotated by an angle  $\theta$  around the  $e_3$ -axis. The final 3D-reconstruction of the sample is then given by applying the inverse Radon transform (with respect to  $y$  and  $\theta$ ) to  $\bar{u}_\theta(y, z)$  for each  $z$ .

### 3 Results

Scans of different tissue phantoms and mouse organs at wavelengths in the visible and near infrared spectrum have been performed, which revealed that a resolution down to  $50 \mu\text{m}$  is achievable. The wavelength of the optical parametric oscillator has to be chosen properly according to the features of interest. The photoacoustic tomography of a mouse heart scanned at 625 nm and 820 nm simultaneously clearly visualizes outer as well as inner structures (see Figs. 4, 5 and 6) and provides best contrast of all used imaging modalities. In this mouse heart almost all heart chambers have collapsed and not all of them are visible on these slices. Image quality is high enough to visualize smaller vessels in the myocardium. The 5 MHz US probe, just like the radiography, could not resolve inner structures of the mouse heart (Figs. 7 and 8). Contrast seems to be satisfactory, but the images appear coarse. Only one cardiac chamber is slightly visible (Fig. 8). Only MRI (Fig. 9) provides comparable image quality concerning tissue differentiation and resolution whereas the contrast is still much higher in photoacoustic images.

Our current results clearly reveal the potential of PAT with integrating line detectors to complement established imaging modalities such as MRT or CT in small animal imaging. Different wavelength allow the representation of any desired structure inside an organ or on the surface. It has been shown elsewhere that the usage of contrast enhancing agents even can enhance image quality and the field of application of PAI.

### 4 Acknowledgements

This work has been supported by the Austrian Science Fund (FWF), projects S10501-N20, S10502-N20 and S10506-N20.

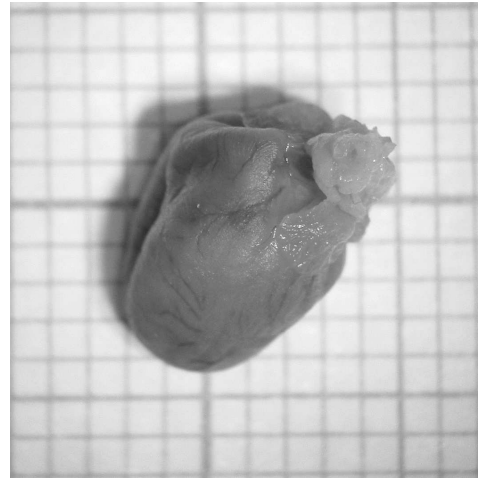


Figure 4: Photo of the mouse heart under investigation, lying on millimeter paper

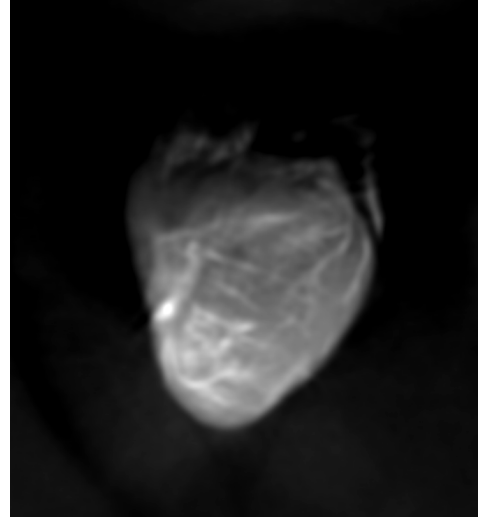


Figure 5: A projection image of the mouse heart with clearly visible vessels on the surface

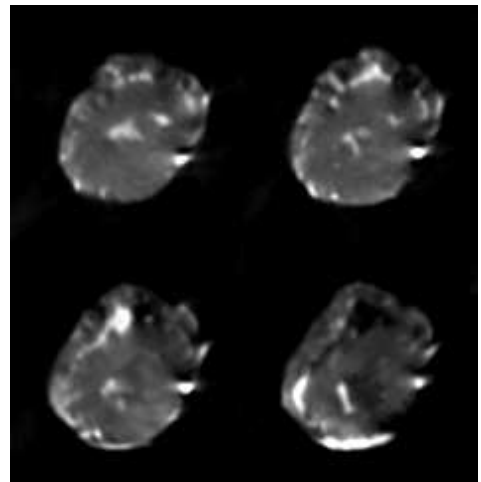


Figure 6: Slices of the tomographic reconstruction of the mouse heart



Figure 7: Mammography of the mouse heart. Almost no inner structures are visible

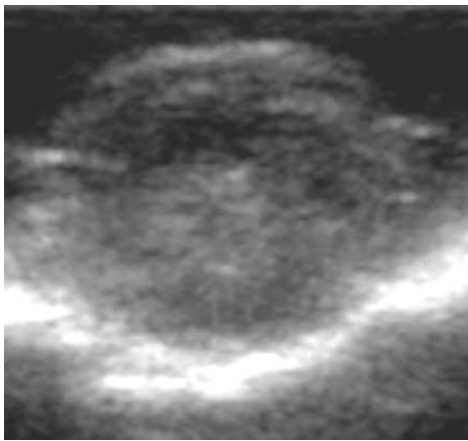


Figure 8: Ultrasonic image of the mouse heart received with a 5 MHz US probe

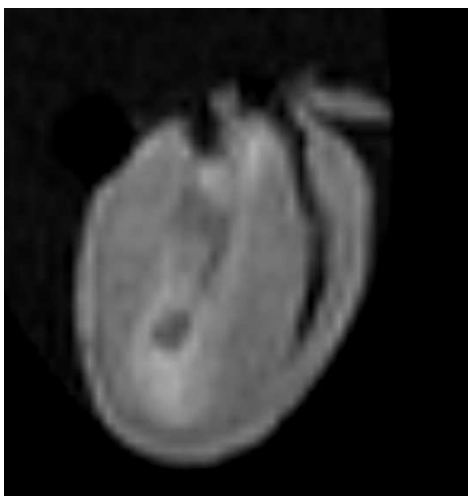


Figure 9: *Four chamber view* of the MRI section of a mouse heart

## REFERENCES

- Burgholzer, P., J. Bauer-Marschallinger, H. Grün, M. Haltmeier, and G. Paltauf (2007). Temporal back-projection algorithms for photoacoustic tomography with integrating line detectors. *Inverse Probl.* 23(6), 65–80.
- Burgholzer, P., C. Hofer, G. Paltauf, M. Haltmeier, and O. Scherzer (2005). Thermoacoustic tomography with integrating area and line detectors. *IEEE Trans. Ultrason., Ferroelectr., Freq. Control* 52(9), 1577–1583.
- Burgholzer, P., G. J. Matt, M. Haltmeier, and G. Paltauf (2007). Exact and approximate imaging methods for photoacoustic tomography using an arbitrary detection surface. *Phys. Rev. E* 75(4), 046706.
- De La Zerda, A., C. Zavaleta, S. Keren, S. Vaithilingam, S. Bodapati, Z. Liu, J. Levi, B. Smith, T. Ma, O. Oralkan, et al. (2008). Carbon nanotubes as photoacoustic molecular imaging agents in living mice. *Nature Nanotechnology*.
- Ewen, K. (1998). *Moderne Bildgebung – Physik, Gertetechnik, Bildbearbeitung und -kommunikation, Strahlenschutz, Qualitätskontrolle*. Stuttgart: Thieme Verlag.
- Haltmeier, M., O. Scherzer, P. Burgholzer, R. Nuster, and G. Paltauf (2007). Thermoacoustic tomography & the circular Radon transform: Exact inversion formula. *Math. Models Methods Appl. Sci.* 17(4), 635–655.
- Heywang-Köbrunner, S. H. and I. Schreer (2003). *Bildgebende Mammadiagnostik – Untersuchungstechnik, Befundmuster, Differentialdiagnose und Interventionen*. Stuttgart: Thieme Verlag.
- Hristova, Y., P. Kuchment, and L. Nguyen (2008). Reconstruction and time reversal in thermoacoustic tomography in acoustically homogeneous and inhomogeneous media. *Inverse Problems* 24(5), 055006 (25pp).
- Köstli, K. P., M. Frenz, H. Bebie, and H. P. Weber (2001). Temporal backward projection of optoacoustic pressure transients using fourier transform methods. *Phys. Med. Biol.* 46, 1863–1872.
- Kruger, R. A., P. Lui, Y. R. Fang, and R. C. Appledorn (1995). Photoacoustic ultrasound (PAUS)—reconstruction tomography. *Med. Phys.* 22(10), 1605–1609.
- Paltauf, G., R. Nuster, M. Haltmeier, and P. Burgholzer (2007a). Experimental evaluation of reconstruction algorithms for limited

- view photoacoustic tomography with line detectors. *Inverse Probl.* 23(6), 81–94.
- Paltauf, G., R. Nuster, M. Haltmeier, and P. Burgholzer (2007b). Thermoacoustic computed tomography using a mach-zehnder interferometer as acoustic line detector. *App. Opt.* 46, 3352–3358.
- Scherzer, O., M. Grasmair, H. Grossauer, M. Haltmeier, and F. Lenzen (2009). *Variational Methods in Imaging*, Volume 167 of *Applied Mathematical Sciences*. New York: Springer.
- Thelen, M. (2007). *Bildgebende Kardiagnostik mit MRT, CT, Echokardiographie und anderen Verfahren*. Stuttgart: Thieme Verlag.
- Wang, Y., X. Xie, X. Wang, G. Ku, K. Gill, D. O’Neal, G. Stoica, and L. Wang (2004). Photoacoustic tomography of a nanoshell contrast agent in the in vivo rat brain. *Nano Letters* 4(9), 1689–1692.
- Xu, M. and L. V. Wang (2006). Photoacoustic imaging in biomedicine. *Rev. Sci. Instruments* 77(4), 1–22. Article ID 041101.